INSTITUTE FOR FUSION STUDIES

DOE/ET-53088-357 IFSR #357

A Fluid-Ion and Particle-Electron Model for Low-Frequency Plasma Instabilities

P.M. Lyster and *J.-N. Leboeuf* *
Institute for Fusion Studies
The University of Texas at Austin
Austin, Texas 78712

**Oak Ridge National Lab.*

January 3, 1989

THE UNIVERSITY OF TEXAS

AUSTIN

A Fluid-Ion and Particle-Electron Model for Low-Frequency Plasma Instabilities

P.M. Lyster
Institute for Fusion Studies
The University of Texas at Austin
Austin, Texas 78712
and
J.-N. Leboeuf
Oak Ridge National Laboratory
Oak Ridge, TN 37830

Shearless!

Abstract

We have developed a hybrid computer code for the study of quasi-neutral electrostatic plasma micro-instabilities. The ions are treated in the fluid approximation, retaining perpendicular $\mathbf{E} \times \mathbf{B}$ and polarization drifts as well as the parallel momentum and ion temperature equations. The particle electrons are treated with perpendicular $\mathbf{E} \times \mathbf{B}$ drifts and parallel kinetics, thus exactly describing the effects of electron-wave resonances. The code is expected to be used in the study of low frequency ($\omega < \Omega_{ci}$) ion-pressure-driven modes and curvature-driven modes. In shearless slab geometry the model has been tested extensively for sound-wave propagation, the universal drift wave real frequency and growth rate, the η_i mode real frequency and growth rate, and the fluctuation spectrum has been elucidated.

A. Introduction

The expression "hybrid code" has come to refer to the use of both particle and fluid simulation models in a single computer code.[1-7] In plasma physics such a technique follows naturally from the fact that plasmas are composed of a number of different charged species: at the most basic level there are electrons present and one species of ion. The large mass ratio $m_p/m_e = 1836$ between protons and electrons contributes to the presence of diverse temporal and spatial scales in the plasma. Ignoring for the moment issues relating to the propagation of electromagnetic radiation, the smallest length is the Debye length $\lambda_D = \sqrt{T_e/4\pi ne^2}$ in cgs units, where T_e is the electron temperature and n is the electron number density, and highest frequency is the plasma frequency $\omega_e = \sqrt{4\pi ne^2/m_e}$. The most natural form of hybrid model is to treat the electrons as a fluid and the ions as particles. This removes kinetic wave-particle electron effects and also removes the $1/\sqrt{N_e}$ noise component, where N_e is a number of electron macroparticles. Also, this allows for further simplification which reduce the scales of applicability. In a sufficiently collisional plasma a simple Ohm's law may be used, or the electron inertia may be neglected in the electron momentum equation. These approximations along with the imposition of quasi-neutrality $n_i = n_e$ eliminate scales of order λ_D and ω_e.[1] Also, the neglect of the electron mass further removes scales of the electron Larmor radius $\rho_e = v_e/\Omega_e$, where v_e is the electron thermal velocity and $\Omega_e = eB/m_e c$ is the electron cyclotron frequency. Furthermore, the Darwin approximation[2] may be imposed whereby the transverse displacement current is neglected and the speed of light on the grid ceases to impose problems of numerical resolution.[3,4,5] The possibilities are many: one quasi-neutral Darwin model due to Hewett and Nielson[6] retains finite electron mass in the longitudinal component oi Ohm's law. Other techniques for increasing the time and space scales exist: amongst these are implicit or time filtering schemes, and orbit averaging or subcycling, and

many of these are discussed in the book "Multiple Timescales."[7]

The hybrid code we are presenting here treats the electrons as particles and the ions as fluid.[8] This is based on the successful theoretical treatments of a number of important modes such as the η_i mode (ion temperature gradient driven)[9,10] or the resistive g mode.[11] In these cases the ions are treated in the fluid approximation, while the electrons are handled with the Boltzman response $n_e = n_0 \exp(e\varphi/T_e)$ where φ is the electrostatic potential. For the relevant modes, quasi-neutrality over scales longer than the Debye length is assumed, the typical frequency ω is taken to be much smaller than the ion Larmor frequency $\Omega_i = eB/m_p c$, and the wavelength λ long compared with the ion Larmor radius $\rho_i = v_i/\Omega_i$. Our model is electrostatic and it retains the electron particle equation of motion in the direction parallel to an ambient magnetic field. We assume vanishingly small electron Larmor radius so that the perpendicular motion can be handled with $\mathbf{E} \times \mathbf{B}$ drifts; this is much in the spirit of Lee and Okuda.[12] Therefore the effects of parallel electron resonances with low frequency electrostatic waves are retained. In the following section the model equations are described and the numerical algorithm outlined. Section C describes extensive tests that were made to verify sound wave propagation, the real and imaginary frequency dispersion relations for the universal mode and η_i mode drift wave modes, and also the fluctuation spectrum properties of the code are elucidated.

B. Model Equations and Algorithm

The ions in the model are treated in the magnetohydrodynamic approximation. The relevant variables are the ion density, the velocity $\mathbf{v}_i$ and temperature T_i. These are related by the equations:[13]

$$\partial_t n_i + \nabla \cdot (n_i \mathbf{v}_i) = 0, \tag{1}$$

$$m_i n_i (\partial_t + \mathbf{v}_i \cdot \nabla)\mathbf{v}_i = e n_i (\mathbf{E} + \mathbf{v}_i \times \mathbf{B}/c) - \nabla P_i - \nabla \cdot \boldsymbol{\pi}_i - \mathbf{R}, \tag{2}$$

$$\frac{3}{2} n_i (\partial_t + \mathbf{v}_i \cdot \nabla) T_i + n_i T_i \nabla \cdot \mathbf{v}_i = -\nabla \cdot \mathbf{q}_i - \boldsymbol{\pi}_i : \partial_{\mathbf{x}} \mathbf{v}_i + Q_i, \tag{3}$$

corresponding to ion continuity, momentum and energy conservation. Here $\mathbf{E} = -\nabla\varphi$ is the electric field, $\mathbf{B}$ is the magnetic field, $P_i = n_i T_i$, $\boldsymbol{\pi}_i$ is the non-isotropic ion stress tensor, $\mathbf{q}$ is the heat flux density, and Q_i is the collisional heating term for ions.

The algorithm is applicable to low frequency $\omega < \Omega_i$ and long wavelength perpendicular to the magnetic field $\lambda_\perp > \rho_i$ microinstabilities. With $\varepsilon = k_\perp \rho_i$ as a small parameter ($k_\perp = 2\pi/\lambda_\perp$) the equation (2) can be expanded in the drift approximation.[14] The ion perpendicular velocity is given by $\mathbf{v}_{\perp i} = \mathbf{v}_{Di} + \mathbf{v}_p$ where

$$\mathbf{v}_{Di} = \frac{c}{B} \hat{b} \times \nabla\varphi + \frac{c}{eBn_i} \hat{b} \times \nabla P_i \tag{4}$$

with the terms on the right-hand side corresponding to the $\mathbf{E} \times \mathbf{B}\,(\mathbf{v}_E)$ and diamagnetic drifts ($\mathbf{v}_{Mi}$) respectively, and

$$\mathbf{v}_p = -\frac{c}{B\Omega_i} (\partial_t + v_{Di} \cdot \nabla) \nabla_\perp \varphi \tag{5}$$

is the ion polarization drift; here $\hat{b} = \mathbf{B}/B$. For the electrons the polarization drift is smaller than the corresponding ion term to $\mathcal{O}(m_e/m_i)$, also we have neglected the contribution from the electron pressure gradient in the present analysis. Thus to the same order as Eq. (4) the perpendicular electron drift is given by $\mathbf{v}_E$.

An equation for the electrostatic potential can be obtained by imposing the quasi-neutrality condition $n_i = n_e\,(\nabla \cdot \mathbf{J} = 0)$. This gives

$$\rho_s^2 \nabla_\perp \cdot (\partial_t + v_{Di} \cdot \nabla) \nabla_\perp \left(\frac{e\varphi}{T_e}\right) = \nabla_\parallel (v_{\parallel i} - v_{\parallel e}), \tag{6}$$

where $\rho_s = c_s/\Omega_i$, $c_s = \sqrt{T_e/m_i}$ and terms on the right-hand side are the parallel derivatives of the ion and electron velocity respectively. Here we have neglected nonlinearities of order $n^{(1)}v_{\|}^{(1)}$ but retained the convective nonlinearity on the left-hand side. The ion description is completed by using simplified versions of the fluid equations for the parallel ion velocity and temperature

$$m_i n_i \left(\partial_t + (\mathbf{v}_E + v_{\|i}\hat{b}) \cdot \nabla\right) v_{\|i} = -e n_i \nabla_{\|}\varphi - \nabla_{\|} P_i \tag{7}$$

$$\frac{3}{2}\left(\partial_t + \left(\mathbf{v}_E + v_{\|i}\hat{b}\right) \cdot \nabla\right) T_i + T_i \nabla_{\|} v_{\|i} = 0. \tag{8}$$

In Eq. (6) the collisional momentum transfer $\mathbf{R}$ between the ion and electron species cancels. The finite Larmor radius part of the ion momentum stress tensor combines with the time derivative of $\mathbf{v}_{Mi}$ in such a way that both terms do not contribute when the quasi-neutrality condition $\nabla \cdot \mathbf{J} = 0$ is applied,[15] also the ion-collision terms in the stress tensor are neglected. In Eqs. (7) and (8) we have taken into account the cancellations between the convective terms and components arising from the stress tensor and the heat flux.[14,16] Also, the nonlinearity in the term $\left(\frac{1}{n_i}\right) \nabla P_i$ in Eq. (7) is neglected in the same spirit as the neglect of the second order density nonlinearity in Eq. (6).

The electrons are treated as macroparticles. The parallel dynamics are followed using the single particle equation of motion, and the perpendicular velocity is $c\mathbf{E} \times \mathbf{B}/B^2$;[12] this is consistent with the derivation of Eq. (6).

$$m_e \frac{d}{dt} v_{\|q} = e \nabla_{\|}\varphi(\mathbf{x}_q), \tag{9}$$

$$v_{\perp q} = \frac{c}{B}\hat{b} \times \nabla\varphi(\mathbf{x}_q), \tag{10}$$

$$\frac{d}{dt}\mathbf{x}_q = \mathbf{v}_{\perp q} + \mathbf{v}_{\|q}, \tag{11}$$

where the subscript q refers to individual particles. The electron parallel velocity that is needed in Eq. (6) and the density $n = n_e = n_i$ in Eqs. (5) and (6) are evaluated using the

subtracted dipole method (SUD)[17]

$$v_{\|e}(x_G) = \sum_q v_{\|q}\, S(\mathbf{x}_G - \mathbf{x}_q) \tag{12}$$

and

$$n_e(\mathbf{x}_G) = \sum_q S(\mathbf{x}_G - \mathbf{x}_q) \tag{13}$$

where S is the particle-grid weighting function for SUD, and $\mathbf{x}_G$ is a grid-point position. The field equations (6)-(8) can then be solved for on a spatial grid.

The geometry is sheared slab. Figure 1 shows a schematic with the "radial" coordinate in usual Tokamak geometry taken to be in the x-direction. The scale lengths for the zero order density and ion-temperature profiles are L_n and L_T respectively. When considering modes driven by ion-temperature-gradient (η_i mode) the quantity $\eta_i = L_n/L_T$ is defined in order to parameterize the the relative scales. The magnetic field is at an angle $\theta(x)$ to the z-axis; when we refer to the shearless case, θ is taken to have no x-dependence. Also, when we refer to the one-dimensional version of the code, only variations in the y-direction are retained. The two-dimensional version has variations in x and y, while for both of the two realizations $k_\| = k_\perp \tan\theta$.

We have normalized Eqs. (6)-(11) according to the following procedure: $t \to \omega_e t$, $\mathbf{x} \to \mathbf{x}/\Delta$ (where Δ is the finite-difference grid spacing), $n \to n/\langle n_0 \rangle$ (where $\langle n_0 \rangle$ is some spatial average of the zero order density), $\mathbf{E} \to (e/m_e\omega_e^2\Delta)\mathbf{E}$, $\varphi \to (e/m_e\omega_e^2\Delta^2)\varphi$, $\mathbf{B} \to e\mathbf{B}/(m_e c\omega_e)$, and $T_i \to T_i/m_e\omega_e^2\Delta^2$. In the new variables the vorticity ($U = \nabla_\perp^2\varphi$), parallel ion momentum, and the ion temperature equations can be rewritten

$$\partial_t U = -\frac{\cos\theta}{B}[\varphi + P, U] - \frac{\cos\theta}{B}[\partial_x P, \partial_x\varphi] - \frac{\cos^3\theta}{B}[\partial_y P, \partial_y\varphi] + \left(\frac{m_e}{m_i}\right) B^2 \nabla_\| (v_{\|i} - v_{\|e}) \tag{14}$$

$$\partial_t v_{\|i} = -\frac{\cos\theta}{B}[\varphi, v_{\|i}] - \nabla_\| v_{\|i}^2/2 - \left(\frac{m_e}{m_i}\right)\nabla_\|\varphi - \left(\frac{m_e}{m_i}\right)\nabla_\| P \tag{15}$$

$$\partial_t T_i = -\frac{\cos\theta}{B}[\varphi, T_i] - v_{\|i}\nabla_\| T_i - \frac{2}{3} T_i \nabla_\| v_{\|i} \tag{16}$$

where $\nabla_{\|} \equiv \sin\theta \frac{\partial}{\partial y}$, $[f,g] = (\partial_x f \partial_y g - \partial_y f \partial_x g)$, and $\tau = T_e/T_i$. In Eq. (4) the linear contribution due to the presence of external density and temperature gradients comes from the Poisson bracket $-(\cos\theta/B)[P,U]$; this contributes a term $(v_D/\tau)(1+\eta_i)\cos\theta\partial_y U$. In Eq. (16) the bracket $-(\cos\theta/B)[\varphi,T_i]$ contributes a term $-(v_D/\tau)\eta_i\cos\theta\partial_y\varphi$, where $v_D = T_e/(BL_n)$ in normalized units.

We now present an outline of the algorithm that is employed. The time advance is performed in two steps, the first of which calculates quantities at a half timestep so that they may be used to advance the equations in a time-centered way. Start with $U^{n+1/2}$, $\varphi^{n+1/2}$, $v_{\|i}^{n+1/2}$, and $T_i^{n+1/2}$ for the ions and $v_{\|q}^n$ and $\mathbf{x}_q^{n+1/2}$ for the electrons; the superscript fixes the time level where $t = n\Delta t$ and Δt is the code timestep. The algorithm is finite-difference in space as well as time, however, the vorticity is inverted using a fast Fourier transform (FFT) to obtain φ. In concert with the SUD particle interpolation scheme we need to filter the grid electron density and parallel velocity. Since the FFT is used to invert the vorticity we perform the filtering in Fourier space with coefficients $\exp -(k^2a^2)$ where a is of the order of the grid spacing.

(a) Ion Half Step

(i) Firstly, calculate the electron velocity at the half step

$$v_{\|q}^{n+1/2} = v_{\|q}^n + (\Delta t/2)e\nabla_{\|}\varphi^{n+1/2}(\mathbf{x}_q^{n+1/2}).$$

Then the velocity moment $v_{\|e}^{n+1/2}$ and density $n_e^{n+1/2}$ can be calculated using Eqs. (12) and (13).

(ii) Advance the vorticity, ion parallel velocity and temperature one half step. From Eqs. (14)-(16) we write

$$U^{n+1} = U^{n+1/2} + (\Delta t/2) f_1\left(U^{n+1/2}, \varphi^{n+1/2}, v_{\|i}^{n+1/2}, v_{\|e}^{n+1/2}\right)$$

$$\varphi^{n+1} = (\nabla_\perp^2)^{-1} U^{n+1}$$

$$v_{\|i}^{n+1} = v_{\|i}^{n+1/2} + (\Delta t/2) f_2\left(v_{\|i}^{n+1/2}, \varphi^{n+1/2}, n_e^{n+1/2}, T_i^{n+1/2}\right)$$

$$T_i^{n+1} = T_i^{n+1/2} + (\Delta t/2) f_3\left(T_i^{n+1/2}, \varphi^{n+1/2}, v_{\|i}^{n+1/2}\right).$$

(b) Ion Full Step

(i) Firstly, advance the electron velocity one full step in a time-centered manner.

$$v_{\|q}^{n+1} = v_{\|q}^{n} + \Delta t\, e \nabla_\| \varphi^{n+1/2}(\mathbf{x}_q^{n+1/2}).$$

Then, in order to calculate $v_{\|e}^{n+1}$ we need to predict $\mathbf{x}_q^{n+1}$

$$\mathbf{x}_q^{n+1} = \mathbf{x}_q^{n-1/2} + (3/2)\Delta t \left\{\mathbf{v}_{\perp q}^{n+1/2} + 0.5(\mathbf{v}_{\|q}^{n+1} + \mathbf{v}_{\|q}^{n})\right\}.$$

(ii) Advance the vorticity one full timestep

$$U^{n+3/2} = U^{n+1/2} + \Delta t\, f_1\left(U^{n+1}, \varphi^{n+1}, v_{\|i}^{n+1}, v_{\|e}^{n+1}\right)$$

$$\varphi^{n+3/2} = (\nabla_\perp^2)^{-1}\, U^{n+3/2}.$$

(iii) Then in order to calculate n_e^{n+1} accurately and to advance the electron position we use a two step process:

$$\mathbf{x}_{q,\mathrm{pred}}^{n+3/2} = \mathbf{x}_q^{n-1/2} + 2\Delta t \left\{\mathbf{v}_{\perp q}^{n+1/2} + 0.5(\mathbf{v}_{\|q}^{n+1} + v_{\|q}^{n})\right\}.$$

This enables us to evaluate $v_{\perp q}^{n+3/2}$ and then,

$$\mathbf{x}_{q,\mathrm{corr}}^{n+1} = \mathbf{x}_q^{n+1/2} + (1/2)\Delta t \left\{\mathbf{v}_{\|q}^{n+1} + 0.5(\mathbf{v}_{\perp q}^{n+1/2} + \mathbf{v}_{\perp q}^{n+3/2})\right\}$$

$$\mathbf{x}_q^{n+3/2} = \mathbf{x}_q^{n+1/2} + \Delta t \left\{\mathbf{v}_{\|q}^{n+1} + 0.5(\mathbf{v}_{\perp q}^{n+1/2} + \mathbf{v}_{\perp q}^{n+3/2})\right\}.$$

(iv) Finally, the ion parallel velocity and temperature are advanced one full timestep

$$v_{\|i}^{n+3/2} = v_{\|i}^{n+1/2} + \Delta t f_2(v_{\|i}^{n+1}, \varphi^{n+1}, n_e^{n+1}, T_i^{n+1})$$

$$T_i^{n+3/2} = T_i^{n+1/2} + \Delta t f_3(T_i^{n+1}, \varphi^{n+1}, v_{\|i}^{n+1}).$$

C. Verification of the Algorithm

The principal tests on the code have involved verifying properties of the real and imaginary frequencies of the linear normal modes, and elucidating the fluctuation spectrum. To evaluate the theoretical estimates of these quantities, we perform a test-current analysis of the linearized equations; much in the spirit of Krall and Trivelpiece.[18] That is, the response potential $\varphi(\mathbf{x},t)$ in Eq. (6) is calculated for an electron current $-ev_{\|}\delta(\mathbf{x}-\mathbf{x}')$ where $\mathbf{x}' = \mathbf{x}_0' + \mathbf{v}_0' t$. Much of the results in this section will pertain to the one-dimensional version of the code, so we perform the analysis retaining only terms with variation in the y-direction. Otherwise the geometry is the same as shown in Fig. 1. The equations will be Fourier transformed in space with the convention $\frac{1}{2\pi}\int dy e^{-iky}$, and Laplace transformed in time according to $\int dt e^{i\omega t}$. The test-current perturbed Eq. (6) is

$$N_0\rho_s^2(\partial_t + v_{Di}\cdot\nabla)\nabla_\perp^2\left(\frac{e\varphi}{T_e}\right) - N_0\nabla_{\|}(v_{\|i}-v_{\|e}) = \nabla_{\|}(v_0/\theta)\delta(y-y') \tag{17}$$

where $v_{\|} = v_0/\theta$ ($\theta \ll 1$) and N_0 is the number density per unit length in the y-direction. The Fourier-Laplace transform is performed and, in what follows, the transient response of the plasma is ignored.

$$N_0\rho_s^2k^2\left(-i\omega + i\omega_{*i}(1+\eta_i)\right)\left(\frac{e\varphi_k}{T_e}\right) + N_0 ik_{\|}(v_{\|i}-v_{\|e}) = \frac{k_{\|}}{2\pi}\left(\frac{v_0}{\theta}\right)\frac{e^{-iky_0'}}{\omega - kv_0'} \tag{18}$$

where $\omega_{*i} = -(T_i/T_e)\omega_{*e} = -kcT_i/eBL_n$. The ion response is calculated using Eqs. (7) and (8)

$$v_{\|i} = \frac{ek_{\|}}{\omega m_i}\varphi_k + \frac{k_{\|}}{\omega m_i}T_i^{(1)} + \frac{T_i k_{\|}}{\omega m_i n_0}n^{(1)} \tag{19}$$

$$T_i^{(1)} = -\frac{\omega_{*i}}{\omega}\eta_i T_e\left(\frac{e\varphi_k}{T_e}\right) + \frac{2}{3}T_i\frac{k_{\|}}{\omega}v_{\|i}. \tag{20}$$

The electron response is calculated by taking the drift-kinetic Vlasov equation

$$\left[\partial_t + \mathrm{v}_{\|}\cdot\nabla_{\mathbf{x}} + \frac{c}{B}\hat{b}\times\nabla\varphi\cdot\nabla_{\mathbf{x}} + \frac{e}{m}\nabla_{\|}\varphi\partial_{v_{\|}}\right]f_e(\mathbf{x},v_{\|},t) = 0 \tag{21}$$

which is appropriate for our model with zero electron Larmor radius, including full dynamics parallel to the magnetic field and $\mathbf{E}\times\mathbf{B}$ drifts in the perpendicular direction. The distribution function is linearized about a maxwellian

$$f_e = f_0 + f^{(1)} \tag{22}$$

where $f_0 = \frac{1}{\sqrt{2\pi}\,v_e}\, e^{-v_\parallel^2/2v_e^2}$, and v_e is the thermal velocity. We evaluate the perturbed distribution function

$$f^{(1)} = \left(\frac{e\varphi_k}{T_e}\right) f_0 \left(1 - \frac{\omega - \omega_{*e}}{\omega - k_\parallel v_\parallel}\right), \tag{23}$$

and then the perturbed electron density and parallel velocity,

$$n^{(1)} = n_0 \int f^{(1)} dv_\parallel = n_0 \left(\frac{e\varphi_k}{T_e}\right) \left(1 - \frac{\omega - \omega_{*e}}{\sqrt{2}\,k_\parallel v_e} Z\left(\frac{\omega}{\sqrt{2}\,k_\parallel v_e}\right)\right), \tag{24}$$

$$v_{\parallel e} = \int f^{(1)} v_\parallel dv_\parallel = \left(\frac{e\varphi_k}{T_e}\right) \frac{\omega - \omega_{*e}}{k_\parallel} \left(1 + \frac{\omega}{\sqrt{2}\,k_\parallel v_e} Z\left(\frac{\omega}{\sqrt{2}\,k_\parallel v_e}\right)\right), \tag{25}$$

where $Z(\xi) = (1/\sqrt{\pi}) \int_{-\infty}^{\infty} dx\, e^{-x^2}/(x - \xi)$ is the Plasma Dispersion Function.[19] Combining Eqs. (18), (19), (20), (24), and (25) we arrive at an expression for the perturbed potential

$$\varphi_k(\omega) = \frac{iT_e k v_0' e^{-iky_0'}}{2\pi e N_0 (\omega - kv_0')\varepsilon(k,\omega)\omega} \tag{26}$$

where

$$\begin{aligned}\varepsilon(k,\omega) = & \left\{k^2\rho_s^2 \left(1 - \frac{\omega_{*i}}{\omega}(1+\eta_i)\right)\right. \\ & - \frac{k_\parallel^2 c_s^2}{\omega^2 - \frac{2}{3}k_\parallel^2 c_s^2/\tau} \left(1 - \frac{\omega_{*i}}{\omega}\eta_i + \frac{1}{\tau}\left(1 + \frac{\omega - \omega_{*e}}{\sqrt{2}\,k_\parallel v_e} Z\right)\right) \\ & \left. + \left(1 - \frac{\omega_{*e}}{\omega}\right)\left(1 + \frac{\omega}{\sqrt{2}\,k_\parallel v_e} Z\right)\right\}. \end{aligned} \tag{27}$$

The dispersion relation $\varepsilon(k,\omega)$ then determines the linear normal modes of the system we are describing. Later, it will be useful to calculate the fluctuating electric field energy spectrum;

we must first evaluate

$$\frac{\langle E^2(y)\rangle}{8\pi} = \frac{N_0}{8\pi}\int dy' \int dv'_{||} f_0(v'_{||}) E(y,y',v'_{||}) E^*(y,y',v'_{||}), \tag{28}$$

where the electric field due to the test current is

$$E(y,y',v'_{||}) = \int \frac{dk}{2\pi} \frac{iT_e k e^{ik(y-y')}}{eN_0\varepsilon(k,kv'_0)}. \tag{29}$$

Writing

$$\frac{\langle E^2(y)\rangle}{8\pi} = \int \frac{dk}{2\pi} W(k),$$

we evaluate the fluctuating energy spectral density

$$W(k) = \frac{T_e^2}{8\pi N_0 \theta e^2} \int_{-\infty}^{\infty} d\omega\, f_0\left(\frac{\omega}{k_{||}}\right) \frac{k}{|\varepsilon(k,\omega)|^2}. \tag{30}$$

(a) Sound Wave Test

The normal modes of the plasma are solutions of the equation $\varepsilon(\omega,k) = 0$. The ion sound wave dispersion relation arises from taking the limit of Z for Boltzmann electrons $|\omega/k_{||}v_e| \ll 1$.

$$Z \approx -\frac{\sqrt{2}\omega}{k_{||}v_e} + i\sqrt{\pi}. \tag{31}$$

With this, and for a homogeneous plasma ($\eta_i = \omega_{*e} = \omega_{*i} = 0$), we get

$$\omega^2 = k_{||}^2 c_s^2 \left(\left(1+\frac{1}{\tau}\right) \Big/ \left(1+k_\perp^2\rho_s^2\right)\right) + \frac{2}{3} k_{||}^2 v_i^2. \tag{32}$$

The first tests on the code were conducted in the limit $\tau \gg 1$, so that for $k_\perp^2\rho_s^2 \ll 1$ we get the usual result $\omega = \pm k_{||}c_s$.

A one-dimensional ($\partial/\partial y \neq 0$) linear (without the convective nonlinearities) version of the code was implemented, and a uniform magnetic field imposed nearly perpendicular to the direction of spatial variation ($\theta = 0.5°$). The timestep was $20\omega_{pe}^{-1}$, and other relevant

quantities were $m_e/m_i = 1/100$, $\Omega_{ce}/\omega_{pe} = 10$, $\tau = 100$. The electrons were initialized with a maxwellian velocity distribution with thermal velocity $v_e = 1.5$ and 2.5. There were 512 gridpoints and 40 simulation particles for gridpoints were used, although good results can be obtained with somewhat less than this number. The numerical stability of the code is mainly determined by the electron streaming condition $k_{\|\max} v_e \Delta t < 1$. This determines the choice of θ, v_e, and Δt; for the above parameter $k_{\|\max} v_e \Delta t = 1.5$ for ($v_e = 2.5$) so for the tests we are operating at the limit of stability. The main reason for pushing this limit is to obtain a long enough time sample in order to resolve the sound wave frequencies. In the code units that were described in Section A ($\omega_{pe}\Delta$ for velocity and Δ for length, where Δ is the grid spacing), we have $c_s = 0.15$ and $\rho_s = 1.5$ (for $v_e = 1.5$), and $c_s = 0.25$ and $\rho_s = 2.5$ (for $v_e = 2.5$).

The dispersion relation is found by evaluating the fluctuation spectrum $W(k, \omega)$ of the homogeneous plasma. Intuitively, it can be seen in Eq. (30) that this quantity peaks at the zeroes of the dispersion relation. For $c_s = 0.25$, and mode number 15 ($k_\perp = 0.184$, or $k_\| = 1.606 \times 10^{-3}$), Figure 2 is a plot of the W as a function of ω, showing distinct peaks close to $\pm k_\| c_s = \pm 4.02 \times 10^{-4}$. Figure 3 shows the frequency plotted against $k_\|$ for $c_s = 0.15$ ($\bullet$), and $c_s = 0.25$ ($\times$). The curves also show the theoretical result obtained from an exact solution of Eq. (27). That the small $k_\|$ behavior satisfies $\omega \approx \pm k_\| c_s$ indicates that the kinetic electrons have Boltzmann-like behavior ($n_e/n_0 = e\varphi/T_e$) in the appropriate regime. The asymptote at high wavenumber can be obtained from the dispersion relation in the limit $k_\perp^2 \rho_s^2 \gg 1$; in that case it is $\omega = \pm(k_\|/k_\perp)\Omega_i = \pm 8.727 \times 10^{-4}$, and this is clearly shown in Figure 3.

(b) The Universal Drift-Wave Test

For the second test we reproduced the universal drift wave instability in shearless ($k_\|/k_\perp =$ const.) geometry. In this case a density gradient inhomogeneity along with finite electron

temperature provides the free energy for a growing electrostatic wave with $k_\parallel/k_\perp \ll 1$. The dispersion relation is established theoretically by retaining the ω_{*e} term in Eq. (27), and substituting both the real and imaginary parts of Z where $|\omega/k_\parallel v_e| \ll 1$ from Eq. (31). Then in the limit $\tau \gg 1$,

$$\varepsilon = k_\perp^2 \rho_s^2 - \frac{k_\parallel^2 c_s^2}{\omega^2} + \left(1 - \frac{\omega_{*e}}{\omega}\right)\left(1 + i\sqrt{\frac{\pi}{2}}\,\frac{\omega}{k_\parallel v_e}\right). \tag{33}$$

Next write $\varepsilon = \varepsilon_1 + i\varepsilon_2$, and the real frequency of the mode is obtained approximately from $\varepsilon_1 = 0$, that is

$$\omega^2(1 + k_\perp^2 \rho_s^2) - \omega\omega_{*e} - k_\parallel^2 c_s^2 = 0. \tag{34}$$

This is the standard form; for example Kadomtsev[20] Eq. (IV.37). There are two solutions which asymptote to the sound wave $\omega = \pm k c_s$ for large values of $k_\parallel c_s$. For $|k_\parallel c_s| < \omega_{*e}$ the positive frequency solution is relevant,

$$\omega_k = \omega_{*e}/(1 + k_\perp^2 \rho_s^2). \tag{35}$$

The growth rate for this mode can be approximated from $\gamma = -\varepsilon_2/(\partial\varepsilon_1/\partial\omega)$ for $\omega = \omega_k$; this gives

$$\gamma = \sqrt{\frac{\pi}{2}}\,\frac{\omega_{*e}^2}{k_\parallel v_e}\,\frac{k_\perp^2 \rho_s^2}{(1 + k_\perp^2 \rho_s^2)^3}, \tag{36}$$

corresponding to Eq. (8.16.11) as derived by Krall and Trivelpiece.[18]

Physically, the universal mode grows due to the interplay between the wave electric field $\mathbf{E}$ and the $\mathbf{E} \times \mathbf{B}_0$ convection of the plasma perpendicular to the density gradient. The result is to increase the population of electrons that travel parallel to the magnetic field resonant with the wave ($v_{\parallel q} = \omega/k_\parallel$), and whose phase is such that $-e v_{\parallel q} \cdot \mathbf{E}_\parallel > 0$; that is, electrons which transfer energy to the wave. The electrons for which $-e v_{\parallel q} \cdot \mathbf{E}_\parallel < 0$ are depleted. In a one-dimensional simulation, only the y-direction is kept, so that the density inhomogeneity must be imposed externally. We employed a scheme in the spirit of the multiple scale approach of Lee[21] except in our case we will apply it to the electron continuity equation

only. The scheme is motivated by noting that the important electron density perturbation due to $\mathbf{E} \times \mathbf{B}$ convection can be written,

$$\partial_t n_e = -\mathbf{v}_E \cdot \nabla n_0 = \frac{n_0 c}{B_0} \hat{b} \times \nabla\varphi \cdot \hat{x}/L_n = \frac{n_0 c}{B_0} \nabla \cdot b \times \varphi\hat{x}/L_n \tag{37}$$

where $\nabla n_0 = -\hat{x} n_0/L_n$, and in slab shearless geometry $\nabla \times \hat{b} = \nabla \times \hat{x}/L_n = 0$. Therefore, since the last expression in (37) is in continuity form the same perturbation can be affected by adding a term $\mathbf{v}_f$ to the electron characteristic velocity

$$\mathbf{v}_{\perp q} = \mathbf{v}_f \triangleq \frac{c}{B_0} \hat{b} \times \varphi\hat{x}/L_n. \tag{38}$$

Note that in a two-dimensional simulation the expression would be $\mathbf{v}_{\perp q} = \mathbf{v}_E + \mathbf{v}_f$.

Figure 4(a) shows the real frequency, obtained once again from the fluctuation spectrum as a function of $k_\perp$. This is done for two different values of $\rho_s/L_n = 0.035$ ($\times$), and 0.75 ($\bullet$). Also, $B = 10$, $v_e = 2.5$, $\omega_{pe}\Delta t = 10.0$, $\tau = 100$ and $m_e/m_i = 1/100$ in normalized units. The numerical solutions of the full dispersion relation Eq. (27) are shown also. Note that the trailing off of the values for large $k_\perp$ probably arises from finite particle effects. For these runs the filtering width was $a = 1.5\Delta$.

The growth of the mode is manifest as an increasing electrostatic field energy. The growth rate, for $\rho_s/L_n = 0.175$, is shown in Figure 4(b) as a function of θ in degrees of arc. The peak occurs for $\theta \approx 0.50$. An estimate for the value can be obtained from the electron-wave resonance condition $\omega_{*e}/k_\| v_e = 1$; from this we get the condition $(k_\|/k_\perp) = (\rho_s/L_n)\sqrt{m_e/m_i}$, or $\theta \approx 1°$. Once again the theoretical result from the dispersion relation is shown. The main significance of this test is that the kinetic wave-particle resonance in the universal mode is well represented by the code.

(c) The η_i Mode

We now consider the situation where both density and temperature gradients are present in the system. In this define $\eta_i = L_n/L_T$ as a measure of the relative magnitude of the tempera-

ture gradient drive compared with the density gradient. Once again take the approximation $|\omega/k_{\|}v_e| \gg 1$ for the electrons, then the dispersion relation (27) becomes

$$\varepsilon = k_{\perp}^2\rho_s^2\left(1 - \frac{\omega_{*i}(1+\eta_i)}{\omega}\right) - \frac{k_{\|}^2c_s^2}{\omega^2 - \frac{2}{3}k_{\|}^2c_s^2}\left(1 + \frac{1}{\tau} - \frac{\omega_{*i}\eta_i}{\omega}\right) + 1 - \frac{\omega_{*e}}{\omega}. \tag{39}$$

This can be solved analytically in several extreme regimes. For $k_{\perp}^2\rho_s^2 \ll 1$, $|\omega_{*i}\eta_i| > |\omega|$, and $|\omega| > |\omega_{*e}|$, which we can regard as the $\eta_i \gg 1$ regime, the solution is $\omega^3 = -k_{\|}^2c_s^2\omega_{*i}\eta_i + (2/3)k_{\|}^2v_i^2\omega$. Neglecting the second term for $\tau \gg 1$ we have[22]

$$\omega = (-k_{\|}^2c_s^2\omega_{*i}\eta_i)^{1/3}. \tag{40}$$

In our geometry $\omega_{*i} < 0$ so that the pole with the positive growth rate is $\omega = (-1 + \sqrt{3})/2|k_{\|}c_s|^{2/3}|\omega_{*i}\eta_i|^{1/3}$. For the case where $|\omega| < |\omega_{*e}|$, or $\eta_i \lesssim 1$ the solution is

$$\omega = k_{\|}c_s\left(\left(\frac{2}{3} - \eta_i\right)\Big/\tau\right)^{1/2}. \tag{41}$$

This root will have a growing part for $\eta_i > \eta_{\rm crit} = 2/3$. When $|\omega_{*i}\eta_i| < |\omega|$ the situation reverts back to that which was described in the previous section. Thus, when $|\omega_{*e}| < |k_{\|}c_s|$ there are three roots $\omega = 0, \pm k_{\|}c_s$, the latter corresponding to the sound wave, and when $|\omega_{*e}| > |k_{\|}c_s|$ the unstable branch is the universal drift mode.

Next consider the case of finite $k_{\perp}^2\rho_s^2$. The important new contribution comes from the term $k_{\perp}^2\rho_s^2\omega_{*i}(1+\eta_i)/\omega$ which is traceable back to the term $\mathbf{v}_{Di}\cdot\nabla$ in the polarization drift (due to the inclusion of finite ion mass) in Eq. (6). When this term is greater than unity the solution to Eq. (39) is $\omega = \pm(k_{\|}/k_{\perp})\Omega_i$, so the η_i mode instability is shut off and the same asymptote is reached as for the ion sound wave. A crude approximation for when the above term becomes important, and thus the largest growth rate is[11]

$$k_{\perp}\rho_s \approx 1/\sqrt{1+\eta_i}\,. \tag{42}$$

The value of $k_{\|}/k_{\perp}$ for the highest growth rate may be estimated by considering when the sound wave frequency approaches the solution (40); thus

$$k_{\|}/k_{\perp} = \eta_i\rho_s/L_n. \tag{43}$$

This is somewhat larger than the value $(\rho_s/L_n)\sqrt{m_e/m_i}$ for the universal drift mode, and is indicative of the diminished role that electron-wave resonance plays in the η_i mode. For typical parameters $\rho_s/L_n = 0.175$, $\eta_i = 2.$, $\rho_s = 2.5$, $m_e/m_i = 1/100$, and $\tau = 1.$, this estimate gives $\theta = 20°$, whereas the optimum angle found from an exact solution of the dispersion relation is $\theta = 6°$. Combining Eqs. (40), (42) and (43) the largest growth rate can be estimated

$$\gamma \sim \frac{\sqrt{3}}{2}(c_s/L_n)\sqrt{\eta_i + 1}\ . \tag{44}$$

This turns out to be about five times too large for the values quoted.

It is instructive to consider schematically the locus of the roots of $\varepsilon(k,\omega)$ in the complex frequency plane. Figure 5(a) shows how the poles move, for small $k_\perp, \rho_s$, as η_i is increased from zero ($\times$) to a number $\eta_i > 2/3$ (o). In the former case the poles line up on the real axis. At $\eta_i = 2/3$ two of the roots are very close to the origin, the third being the universal drift root. For $\eta_i > 2/3$ the familiar triad corresponding to Eq. (40) is reached. Figure 5(b) then shows the locus of the poles as $k_\perp \rho_s$ is increased. The most significant trend is that the imaginary frequency of the η_i mode root increases and then falls in accord with the above discussion.

The real frequency part of the dispersion relation was tested in the same way as in the previous sections, using the fluctuation spectrum. A long time sample is needed in order to pick up the real frequency, so we took $\eta_i = 2/3$, that is, at marginal stability. The other parameters were $\rho_s/L_n = 0.011$, $\rho_s = 1.5$, $\theta = 0.5°$, and $\tau = 1$. Figure 6(a) shows the plot of ω_r versus $k_\perp$. The two curves show the two roots (refer to Fig. 5(a)) with negative real frequency. Superimposed on these waves are the points obtained from the fluctuation spectra, showing significant discrepancy at high $k_\perp$ due to finite particle size effects. Figure 6(b) shows the growth rate versus $k_\perp$ for $\rho_s/L_n = 0.175$, $\rho_s = 2.5$, $\eta_i = 16$, $\theta = 6°$, $m_e/m_i = 1/100$, and $\tau = 1$. The curve is obtained from the exact solution of the dispersion relation, while

the points are obtained by running the one-dimensional code. It was necessary to impose an initial perturbation on the parallel ion velocity ($\approx 0.1 v_i$) in order to observe this instability. This was done at the various values of $k_\perp$ for which the points are parallel in the figure.

(d) The Fluctuation Spectrum

One important test of a code is to compare the fluctuation spectrum for a homogeneous stable plasma with the theoretical expression Eq. (30). A closed form for the frequency integral could not be obtained, however, we can estimate the result by taking the high frequency approximation of the dispersion relation. In the limit $|\omega/\sqrt{2}\, k_\parallel v_e| \gg 1$

$$Z \approx \frac{\sqrt{2}\, k_\parallel v_e}{\omega} - \sqrt{2}\left(\frac{k_\parallel v_e}{\omega}\right)^3 + i\sqrt{\pi}\exp\left[-(\omega/\sqrt{2}\, k_\parallel v_e)^2\right], \tag{45}$$

and writing

$$\varepsilon(k,\omega) = \varepsilon_1 + i\varepsilon_2$$

we have

$$\varepsilon_1 = k^2\rho_s^2\left(1 - \frac{\theta^2\Omega_e\Omega_i}{\omega^2}\right)$$

$$\varepsilon_2 = \sqrt{\frac{\pi}{2}}\frac{\omega}{k_\parallel v_e}\exp\left[-(\omega/\sqrt{2}\, k_\parallel v_e)^2\right]. \tag{46}$$

The high frequency root is approximately given by $\omega_k = \pm\theta\sqrt{\Omega_e\Omega_i}$. The contribution to the argument of Eq. (30) can be estimated by expanding ε about ω_k.[23]

$$\mathrm{Im}\,\frac{1}{\varepsilon} \approx \frac{\pi}{\frac{\partial\varepsilon_1}{\partial\omega_k}}\left[\delta\left(\omega + \theta\sqrt{\Omega_e\Omega_i}\right) + \delta\left(\omega - \theta\sqrt{\Omega_e\Omega_i}\right)\right]. \tag{47}$$

With this the integral Eq. (14) can be performed

$$W(k) = \frac{1}{2}\left(\frac{v_A}{c}\right)^2 T_e \tag{48}$$

where $v_A = B^2/\sqrt{4\pi\, m_i N_0}$. This expression reveals the low-noise nature of the code. When the fluctuations are dominated by the plasma frequency the factor $(v_A/c)^2$ is not present.

Three test runs were performed; the common parameters were $v_e = 1.5$, $\theta = 0.5$, $\omega_{pe}\Delta t = 5.$, and $\tau = 100.$. For case (a) $m_e/m_i = 1/100$, $B = 10$, that is $(v_A/c) = 1$; case (b) $m_e/m_i = 1/1600$, $B = 10$, that is $(v_A/c) = 1/4$; and case (c) $m_e/m_i = 1/100$, $B = 1$, that is $(v_A/c) = 1/10$. Figure 7 shows the log plots of the normalized spectrum $W'(k) = W(k)/\left((n_0/N_0)T_e/2\right)$ for the respective cases (a), (b) and (c). For reference the curves $(v_A/c)^2/(1 + k_\perp^2\rho_s^2)$ are plotted along with the numerical points. The asymptotes at $k_\perp\rho_s \to 0$ and the behavior of finite $k_\perp\rho_s$ seem to be well represented up to the point where finite particle size effects play a role.

D. Conclusions

We have developed and tested a new computer algorithm for the study of low-frequency plasma instabilities. The electric field is obtained from the quasineutrality condition. Here the important physics comes from the perpendicular polarization drift, due to the finite mass of the ions; through the continuity equation this drift is balanced by the parallel motion of both ions and electrons. The new feature is that the parallel electron motion is treated kinetically so that wave-particle resonance effects are retained. The code was tested for ion sound wave propagation, and it gave the correct linearized η_i mode dispersion properties. These are important tests for the fluid-ion and Boltzman-electron properties in regimes where they should apply. We also tested for the universal mode dispersion properties; here the kinetic properties of the electrons play an important role. The fluctuation spectrum is proportional to $(v_A/c)^2T_e$ per mode. The factor $(v_A/c)^2$ indicates the low-noise character of the algorithm. Also, the measured spectrum of the code does not exceed the theoretical estimate; only at high wave number k is there some discrepancy due to the particle-grid effects. We not. the use of vorticity equation to obtain the electrostatic potential in terms of the parallel derivative of the current, whereas in conventional electrostatic codes the potential is obtained from poisson's equation. In the future nonlinear applications for the η_i mode in

slab geometry will be performed.

Acknowledgments

We would like to thank B.A. Carreras, P.H. Diamond, G.S. Lee, and P.W. Terry for their assistance in this work. This work was supported by the U.S. Department of Energy under contracts DE-FG05-80ET-53088 with the Institute for Fusion Studies, The University of Texas at Austin, and DE-AC05-84-or 21400 with Martin Marietta Energy Systems, Inc.

References

1. J.A. Byers, B.I. Cohen, W.C. Condit, and J.D. Hanson, J. Comput. Phys., **27**, 363 (1978).

2. C.G. Darwin, Phil. Mag., **39**, 537 (1920).

3. C.W. Nielson, and H.R. Lewis, *Methods in Computational Physics* (Academic, NY) **16**, 367 (1976).

4. A. Mankofsky and R.N. Sudan, J. Comput. Phys. **70**, 89 (1987).

5. D.S. Harned, J. Comput. Phys. **47**, 452 (1982).

6. D.W. Hewett and C.W. Nielson, J. Comput. Phys. **29**, 219 (1978).

7. in *Multiple Timescales*, edited by J.U. Brackbill and B.I. Cohen (Academic, Orlando, 1985).

8. H. Okuda, Space Science Reviews **47**, 41 (1985).

9. G.S. Lee and P.H. Diamond, Phys. Fluids **29**, 3291 (1986).

10. W. Horton, R.D. Estes, and D. Biskamp, Plasma Phys. **22**, 663 (1980).

11. H.P. Furth, J. Killeen, and M.N. Rosenbluth, Phys. Fluids **6**, 77 (1963).

12. W.W. Lee and H. Okuda, J. Comput. Phys. **26**, 139 (1978).

13. S.I. Braginskii, in *Reviews of Plasma Physics*, edited by M.A. Leontovich (Consultants Bureau, NY, 1965), Vol. I, p. 205.

14. S. Tsai, F.W. Perkins, and T.H. Stix, Phys. Fluids **13**, 2108 (1970).

15. F.L. Hinton and C.W. Horton, Jr., Phys. Fluids **14**, 116 (1971).

16. C.W. Horton, Jr. and R.K. Varma, Phys. Fluids **15**, 620 (1972).

17. C.K. Birdsall and A.B. Langdon, *Plasma Physics via Computer Simulation* (McGraw-Hill, NY, 1985).

18. N.A. Krall and A.W. Trivelpiece, *Principles of Plasma Physics* (McGraw-Hill, NY, 1973).

19. B.D. Fried and S.D. Conte, *The Plasma Dispersion Function* (Academic, NY, 1961).

20. B.B. Kadomtsev, in *Plasma Turbulence* (Academic Press, NY, 1965).

21. W.W. Lee, J. Comput. Phys. **72**, 243 (1987).

22. B. Kadomtsev and O.P. Pogutse, in *Reviews of Plasma Physics*, Vol. V, p. 249, (Consultants Bureau, NY, 1970).

23. S. Ichimaru, *Basic Principles of Plasma Physics: A Statistical Approach*, in Frontier in Physics (Benjamin/Cummings, Reading, Massachusetts, 1973).

Figure Captions

1. The schematic sketch of sheared slab configuration.

2. The fluctuation spectrum $W(k,\omega)$ for a homogeneous plasma with $c_s = 0.25$ at $k_{||} = 1.606 \times 10^{-3}$.

3. The sound-wave dispersion relation for $c_s = 0.15$ (O) and 0.25 $(\times)$.

4. (a) Universal drift wave real frequency dispersion relation. (b) Universal drift wave growth rate.

5. (a) locus of roots of dispersion relation in the complex ω-plane for increasing η_i. (b) locus of roots of dispersion relation in the complex ω-plane for increasing $k_\perp$.

6. (a) The η_i mode real frequency dispersion relation. (b) The η_i mode growth rate.

7. The logarithm of the normalized fluctuation spectrum $W'(k)$ for (a) $v_A/c = 1$, (b) $v_A/c = 1/4$, and (c) $v_A/c = 1/10$.

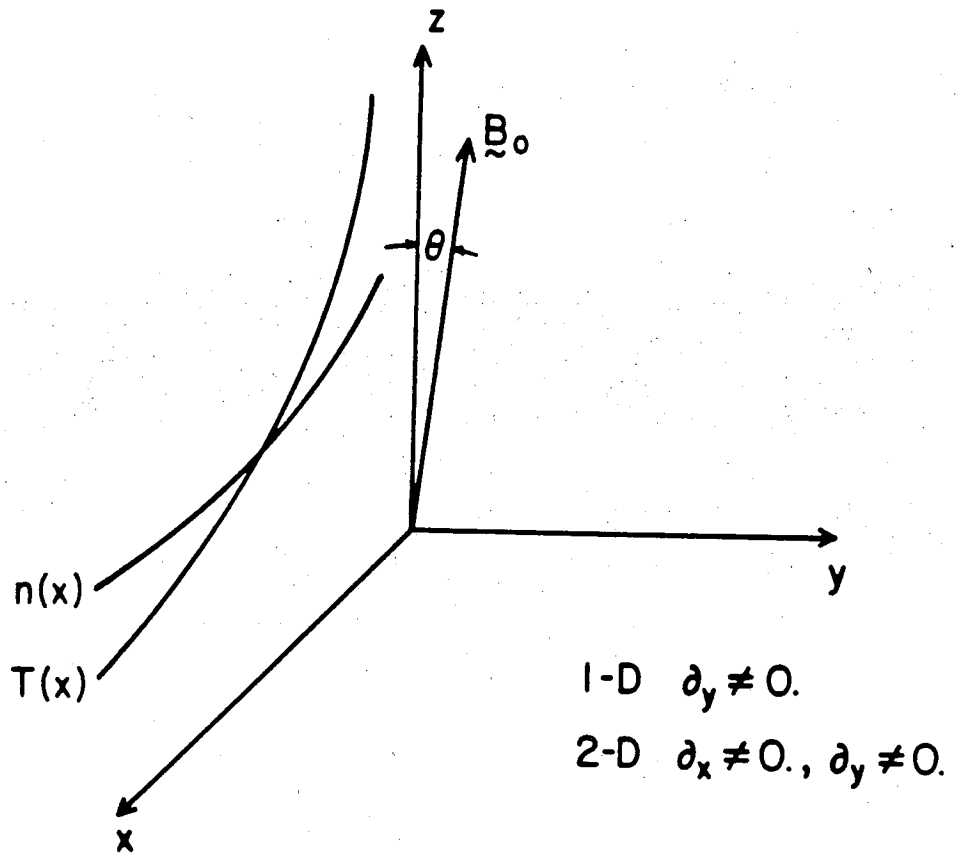

Fig. 1

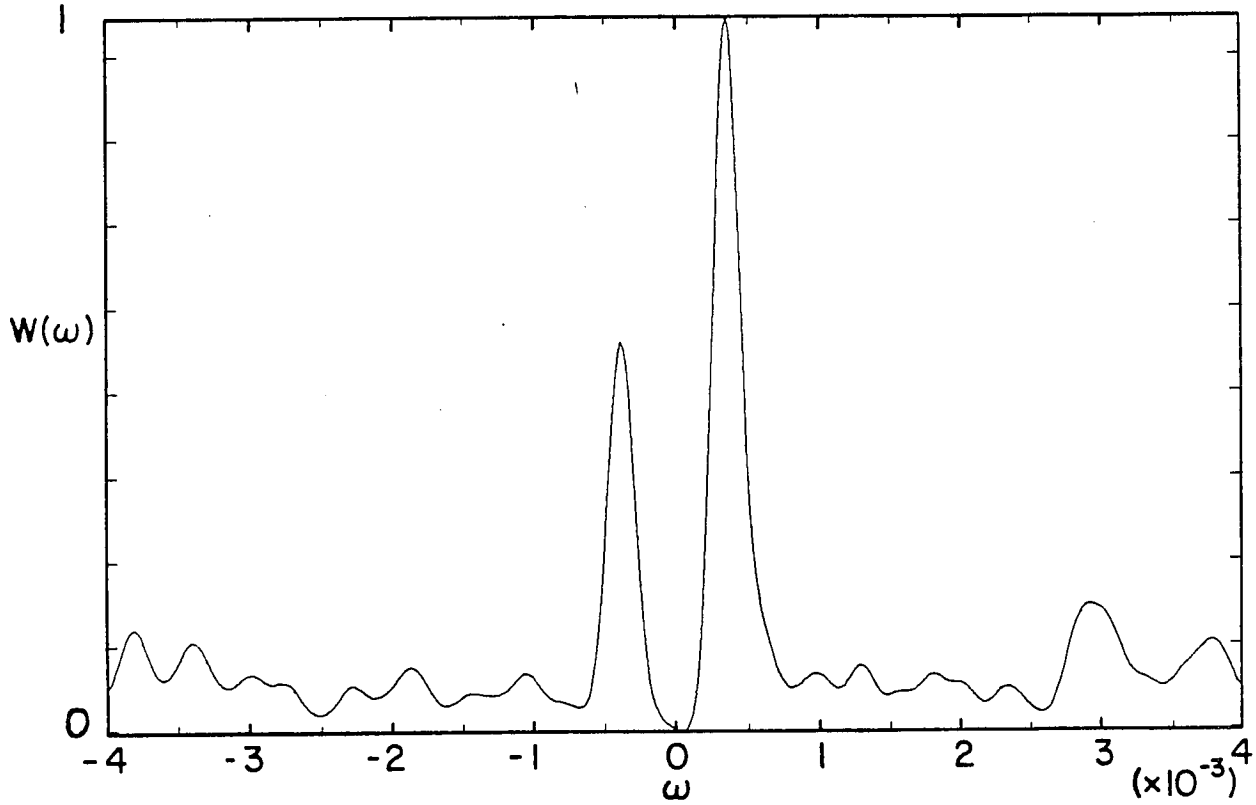

Fig. 2

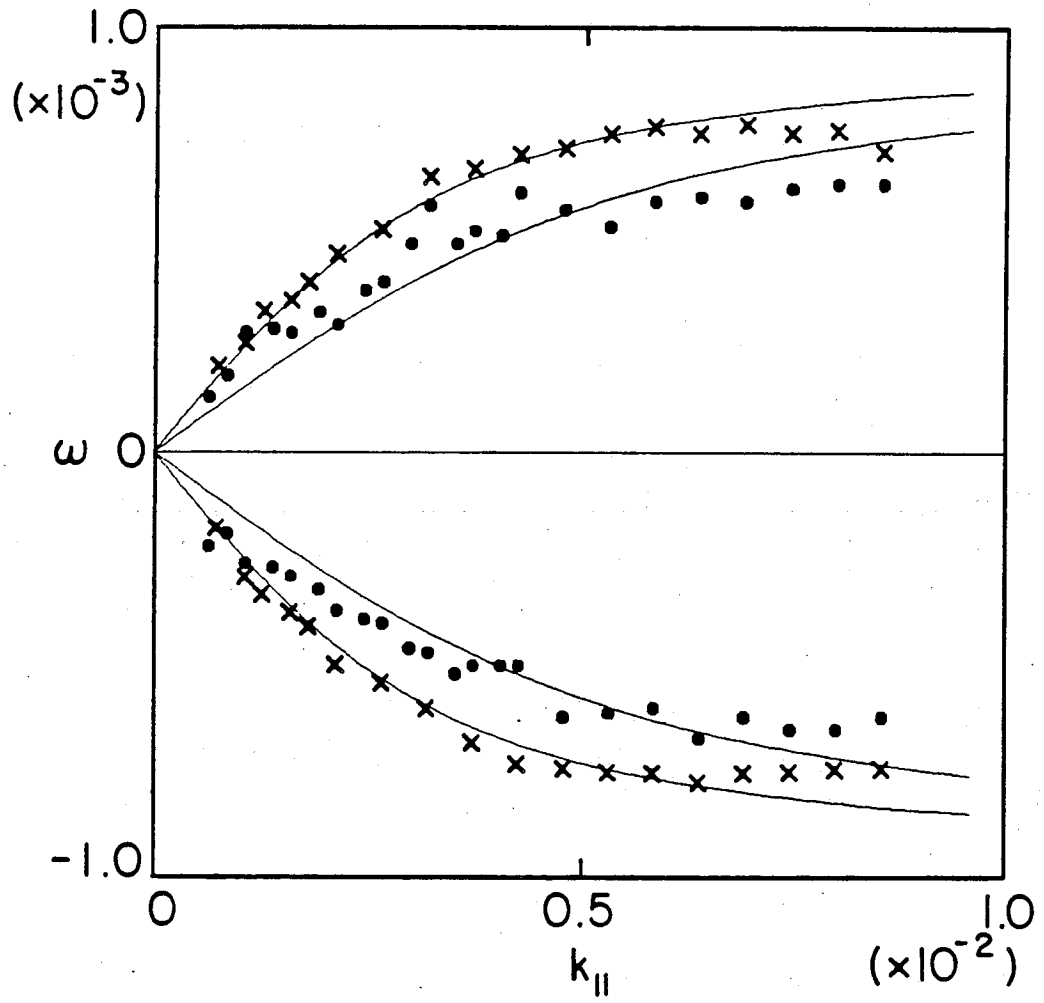

Fig. 3

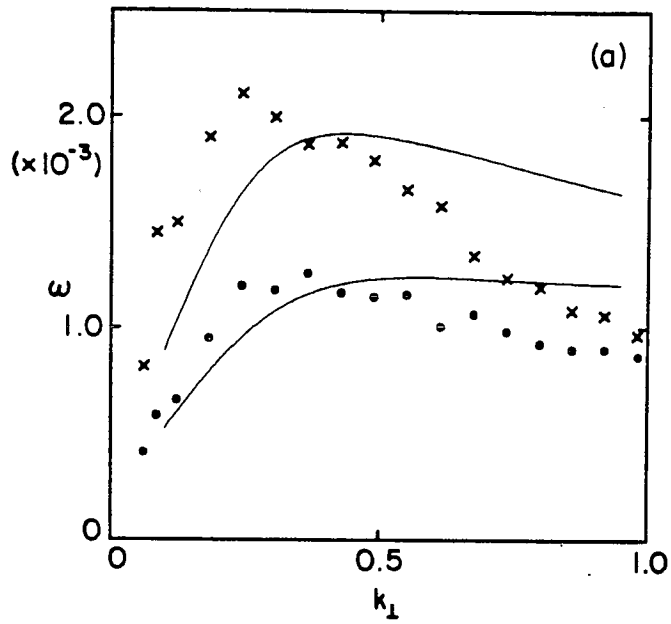

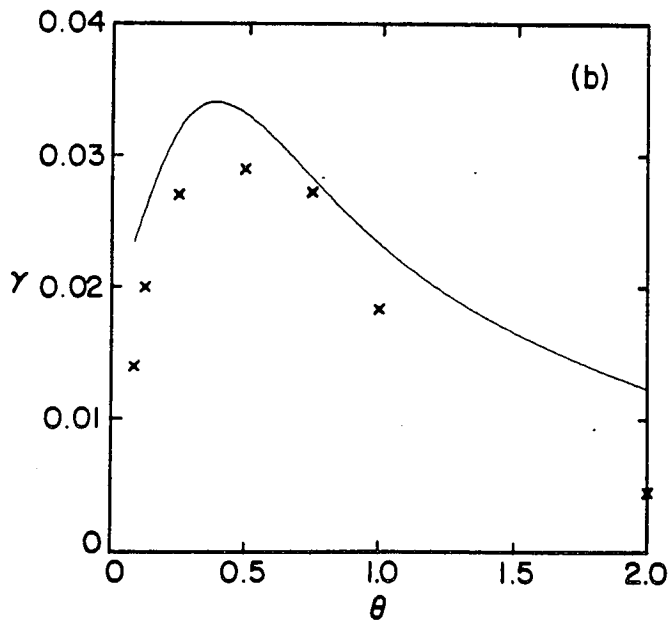

Fig. 4

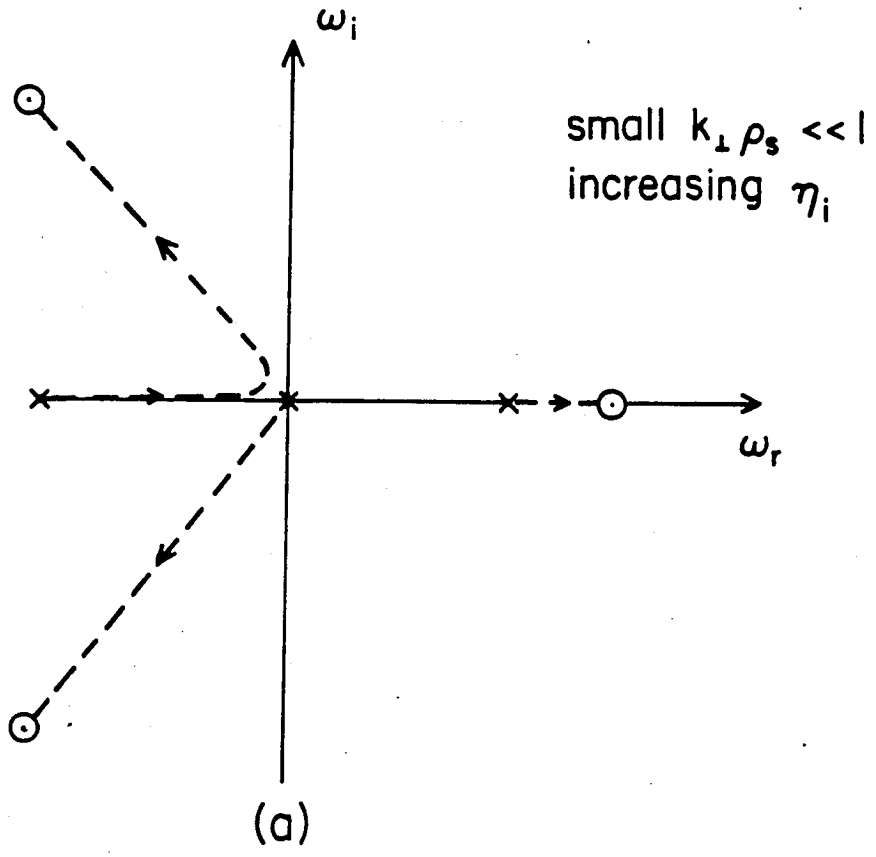
ω_i
small $k_\perp \rho_s << 1$
increasing η_i
ω_r
(a)

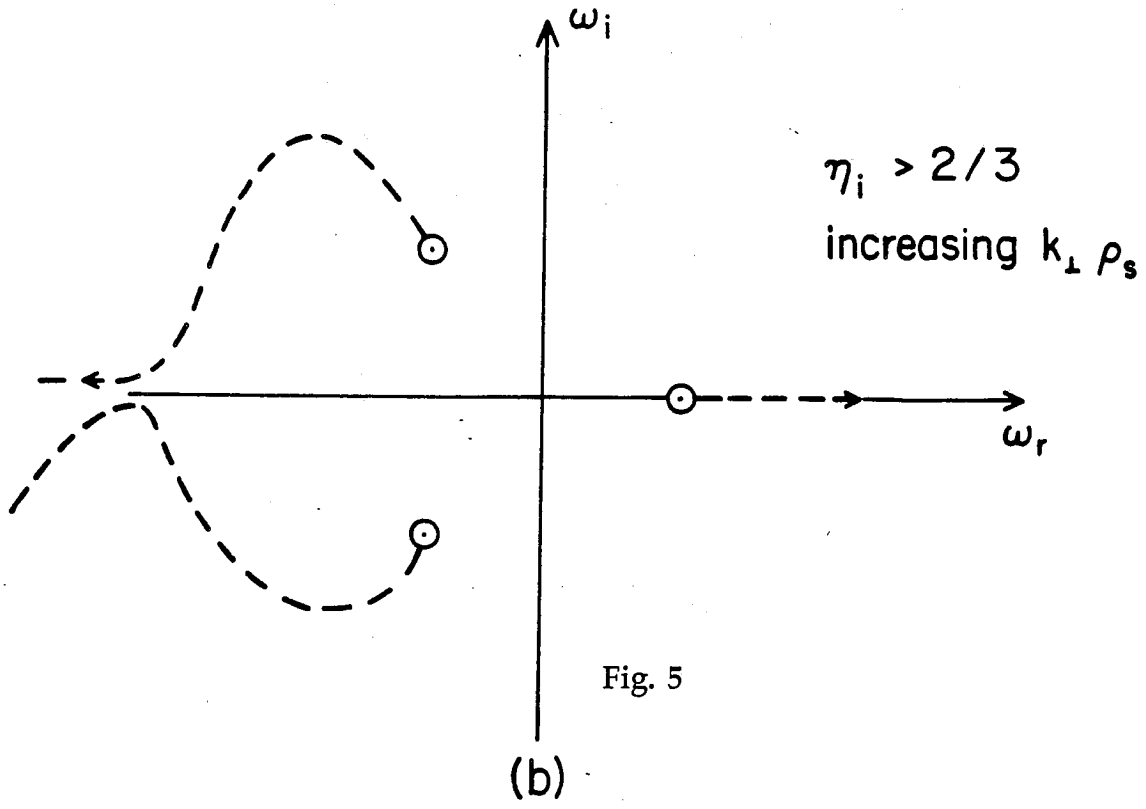
ω_i
$\eta_i > 2/3$
increasing $k_\perp \rho_s$
ω_r
(b)

Fig. 5

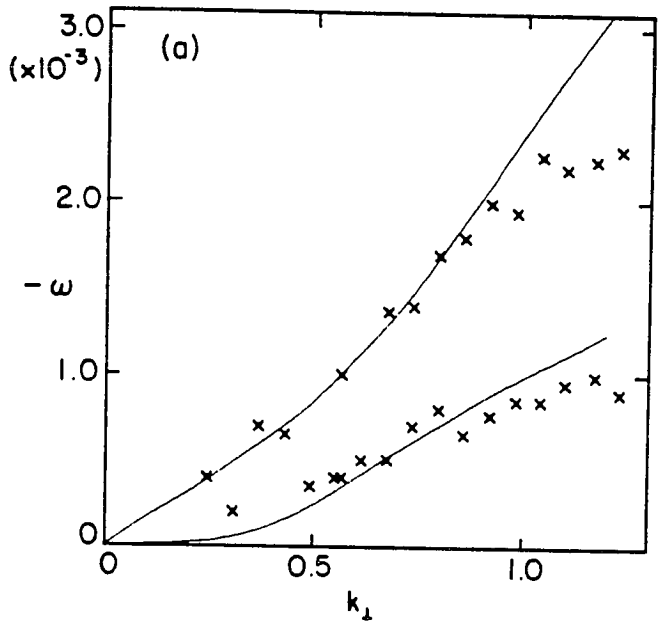

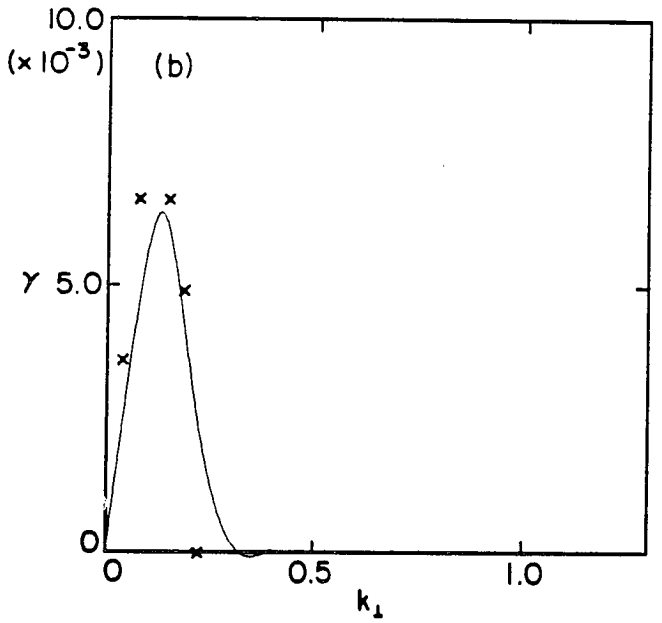

Fig. 6

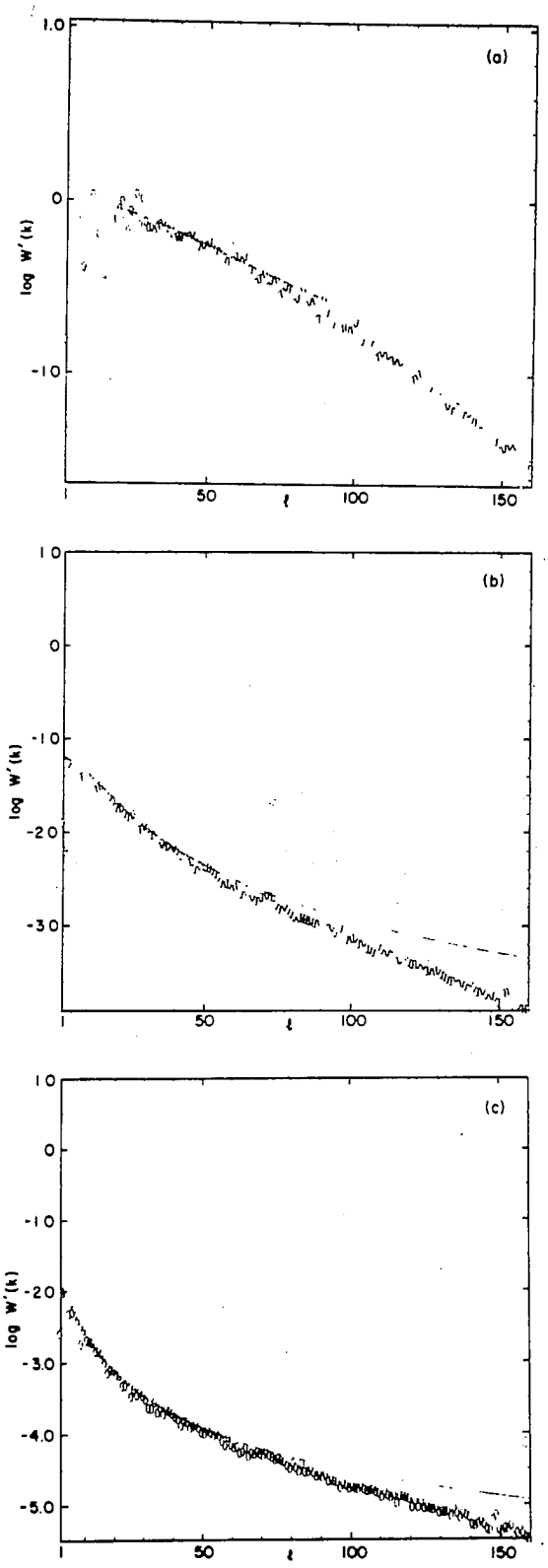
(a)
1.0
0
-10
log W'(k)
1
50
100
150
k
(b)
10
0
-10
-20
-30
log W'(k)
1
50
100
150
k
(c)
10
0
-10
-20
-30
-40
-50
log W'(k)
1
50
100
150
k

Fig. 7